MRS Advances
https://doi.org/10.1557/s43580-026-01710-8

ORIGINAL PAPER

Microstructural examination of Cu-Nb and Cu-Nb-Ag composites

Hannah Matos-Pimentel[1] · Matthew Besser[2] · Ryan Timothy Ott[2] · Ke Han[1]

Received: 3 December 2025 / Accepted: 29 June 2026

Abstract

The manufacture of Cu-Ag and Cu-Nb products begins with solidification. Among the three elements (Cu, Ag, and Nb), the highest melting point is that of Nb. Melting Cu-Nb alloys, therefore, requires very high temperatures. To reduce the melting point, Ag has been considered as a potential melting-point depressant. In this study, we investigated as-solidified Cu-Nb composites with and without Ag addition, and we observed particles with a variety of sizes and geometries. Our data showed that, in as-solidified composites, Nb dendrite formation was significantly affected by the presence of Ag, which later formed smaller particles in the Cu matrix. Furthermore, Nb particles appeared to be separated by Ag particles so that the addition of Ag led to a less homogeneous distribution of Nb dendrites. In this paper, we report our findings on the microstructural distribution of Nb and Ag in our solidified samples, and we discuss the implications of such distribution on the future fabrication of products.

Introduction

Because of their thermal conductivity and mechanical strength, both alloys and composites made from Cu are widely used for applications in aerospace, nuclear fusion, electronic packaging, and high heat flux systems. Copper-based composites in particular are also used in high-field magnets [1, 2]. High-field magnets, which enable experiments under extreme magnetic conditions, are essential for advanced research in the fields of materials science, chemistry, physics, and biology. These magnets require conductors that have high enough mechanical strength to withstand Lorentz forces and high enough electrical conductivity to minimize Joule heating [3–6].

In the US National High Magnetic Field Laboratory (commonly known as MagLab), both Cu-Ag and Cu-Nb composites (in which the Cu matrix is strengthened by either Ag or Nb fibers) are widely used as high-strength conductors. Each composite has advantages and disadvantages: The advantage of Cu-Nb is that, not only is its achievable strength higher than that of Cu-Ag but also its electrical conductivity remains high because of the negligible solubility of Nb in Cu [7–9]. During severe plastic deformation, Nb dendrites, which are formed during casting, are transformed into filamentary ribbons whose tight spacing enables UTS (ultimate tensile strength) exceeding 2 GPa at high strain levels.

One of the disadvantages of Cu-Nb is that the casting of Cu-Nb can be quite difficult because of the high melting point of Nb. At the same time, the wide spacing between Nb dendrites makes it necessary to apply time-consuming fabrication methods—like accumulative drawing or roll bonding—in order to reach extreme deformation strain levels. These methods limit scalability and increase the cost of production [8].

By contrast, Cu-Ag composites can be made by casting at lower temperatures and processing at lower deformation strains [10–12]. The strength of these composites arises largely from 1) the eutectic products formed during solidification and 2) the precipitation hardening that occurs during aging. Aging leads to the formation of Ag precipitates through either discontinuous precipitation or continuous precipitation or both [13–20]. At low deformation strain levels, increasing Ag content enhances strength. Once the Ag content reaches a certain level, however, further enhancement of achievable strength in the composite with higher Ag content falls below that of the composite with lower Ag content.

✉ Ke Han
han@magnet.fsu.edu

[1] National High Magnetic Field Laboratory, Florida State University, Tallahassee, FL 32310, USA

[2] Ames National Laboratory, 2408 Pammel Dr, Ames, IA 50011, USA

Published online: 13 July 2026

Table 1 Summary of composition, phase content, and Nb dendrite geometry in Cu-Nb and Cu-Nb-Ag alloys

	Items	Cu-Nb	Cu-Nb-Ag
Nominal composition and area-based estimation (Image Analysis)	Nb (nominal wt%)	14.7	9.6
	Nb (area%)	21.3	7.9
	Ag (nominal wt%)	–	8.3
	Ag (area%)	–	4.0
Primary casting condition	Voltage (V)	28	28
	current (A)	2000–2200	2200
	Time (minutes)	15.7	13.4
Secondary casting condition	Voltage (V)	28	28
	current (A)	2000	2100
	Time (minutes)	12	12.1
Composition in single phase (EDS)	Nb dendrite (Cu%)	1.8	1.2
	Nb dendrite (Nb%)	98.2	98.8
	Cu matrix (Cu%)	100.0	92.4
	Cu matrix (Ag%)	–	7.6
Geometric description and statistical analyses	Feret diameter average (μm)	12.0	9.9
	Roundness	0.7	0.7
	Circularity	0.7	0.8
	Fractal Dimension (D_b)	1.7	1.5
	r^2 for D_b (Regression Fit Quality)	0.997	0.993
	Lacunarity	0.3	0.7
	Number of particles/dendrites	1650	1208
	Number of dendrites/area (count/μm^2)	0.013	0.015

High Ag content may also reduce electrical conductivity. Researchers have been working on optimization of Ag levels to balance properties and fabrication routes. Previous studies have explored the use of ternary systems to refine precipitates and improve performance. Typical examples are Cu-Ag-Zr composites [21–25] and Cu-Ag-Sc [13–16].

Building on the foundation of Cu-Ag and Cu-Nb, researchers have introduced Nb as a third element in Cu-Ag alloys in order to enhance the mechanical strength. Alternatively, other researchers have introduced Ag as a third element in Cu-Nb alloys in order to reduce the melting point, [8, 18, 26–28]. Cu-8.2wt% Ag-4wt% Nb alloy composites, which were reported a capability to withstand very high drawing strains without annealing, have demonstrated high tensile strength (up to 1.84 GPa) after heavy deformation [26]. After such high drawing strains in a Cu–5 at.% Ag–3 at.%Nb, researchers reported mechanical alloying occurred among Cu, Nb, and Ag and amorphization at some of the Cu–Nb interfaces [8]. The mechanisms behind these enhancements, however, need more studies (particularly those that depend on the synergetic effect of Ag and Nb on precipitation and dendrite formation in ingots). Our findings reveal that Ag-rich regions can nucleate on Nb dendrites, influencing their growth kinetics and potentially altering the microstructural evolution of the composite.

Experimental details

Both Cu-Nb and Cu-Nb-Ag were in cast condition (Table 1). Because we expected that Ag formed finer strengthening particles than Nb, we therefore selected Cu-Nb-Ag ingot with Nb content significantly lower than Cu-Nb. Ingots were cast in two complete melting cycles. CuNb was started as an electrode and cast to an ingot. It was then reduced in diameter and remelted again. Cu-Nb-Ag was also double melted in a similar manner.

Specimens for microscopy were prepared by sectioning the ingots using a low-speed saw. Each specimen was subsequently ground using SiC abrasive papers of progressively finer grit. This was followed by mechanical polishing using diamond suspensions. Final polishing was performed using colloidal silica to minimize mechanical deformation.

Microstructural characterization was conducted using a Thermo Fisher G4 UC Scanning Electron Microscope (SEM) equipped with an energy-dispersive X-ray spectroscopy detector (EDS). The EDS data were acquired at 15 kV and a beam current of 0.8 nA.

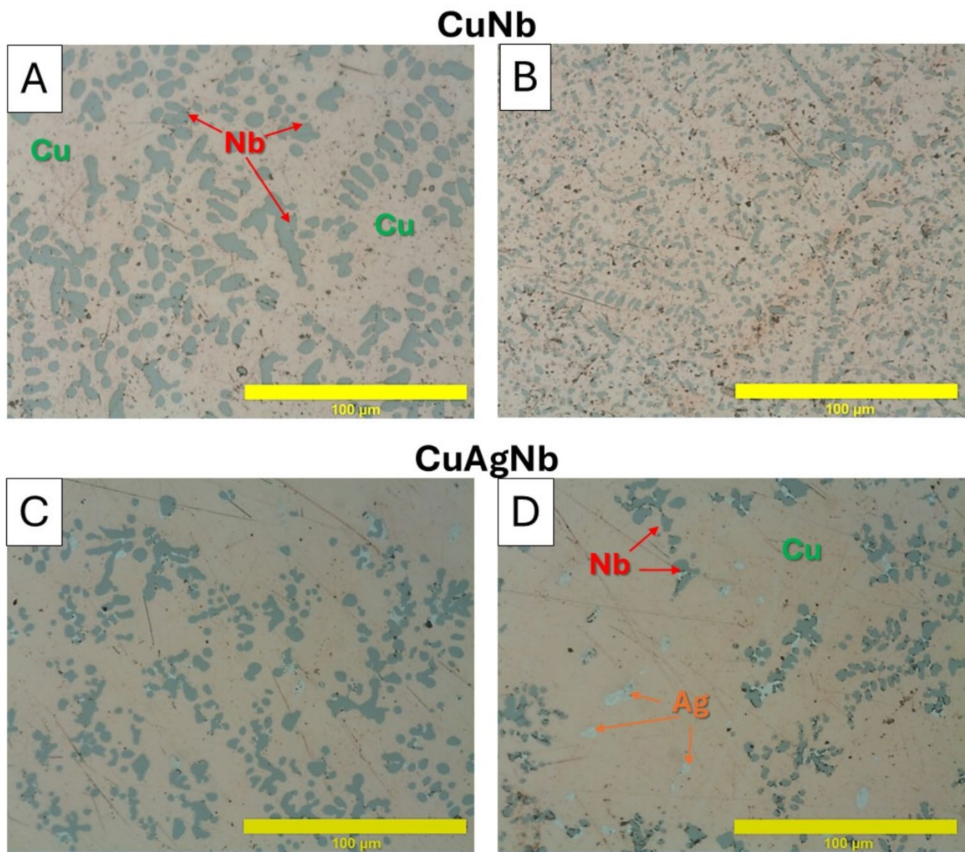

Fig. 1 Light microscopy images of Cu-Nb (**A, B**) and Cu-Nb-Ag (**C, D**) at equal magnification. **A** an image of a Cu-Nb sample with coarse Nb dendrites (gray/green colored particles); **B** an image of a Cu-Nb sample with relatively fine Nb dendrites; **C** an image of a Cu-Nb-Ag sample with coarse Nb dendrites dominating the imaged area; **D** an image of a Cu-Nb-Ag sample with a relatively large volume fraction of Ag (light/white colored particles)

Although our two-dimensional images provide only planar snapshots of features that are inherently three dimensional, statistically analyzing many such 2D sections allows key aspects of the 3D morphology—such as dendrite connectivity, branching complexity, and phase distribution—to be inferred. Metrics like area fraction, fractal dimension, and particle spacing measured in 2D often correlate well with their 3D counterparts under stereological principles. Thus, rigorous 2D image analysis offers a practical and reliable means to understand the 3D solidification structure, even when direct 3D characterization is not feasible. Using the trainable Weka Segmentation plugin in Fiji, image segmentation was performed to identify Nb and Ag particles in samples for statistical analysis [29]. The image analyses were undertaken on accumulated areas of 4.65 mm^2 and 4.33 mm^2 for Cu-Nb and Cu-Nb-Ag, respectively. The numbers of dendrites analyzed exceeded 1200 (Table 1).

Results and discussion

Samples of both ingots showed Nb dendritic structure. Based on the consideration that the area fraction obtained from image segmentation was representative of the volume fraction of Nb and Cu phases, and assuming that the microstructure was isotropic and that the analyzed section was statistically representative, we analyzed the volume fraction of the Nb phase. Our measured volume fraction levels of Nb in Cu-Nb and Cu-Nb-Ag were 21 vol% and 10 vol%, respectively (Table 1). In most areas of the Cu-Nb samples, our images showed coarse Nb dendrites (Fig. 1A). In relatively smaller areas, we observed finer Nb dendrites (Fig. 1B). In most areas in the Cu-Nb-Ag samples, coarse Nb dendrites dominated the imaged areas (Fig. 1C). In relatively small areas, we observed large numbers of components containing Ag particles (Fig. 1D). The Ag particles in our images appeared to have formed independently from Nb dendrites.

In addition to our measured volume fraction levels of Nb in Cu-Nb and Cu-Nb-Ag (Table 1), we also estimated the volume fraction of Ag. In most cases, Ag area content measurement by area fraction was converted to a weight percent between 1 and 4. This value was lower than the nominal 8.3 wt%Ag. Our measurements of this Ag content were derived from the measurements of the features shown in the images. These features were probably from the area in the samples that contained eutectic reaction products; Ag content revealed by light microscope may be even lower. We therefore deduced that a significant amount of Ag was dissolved in Cu at solidification temperatures. As the

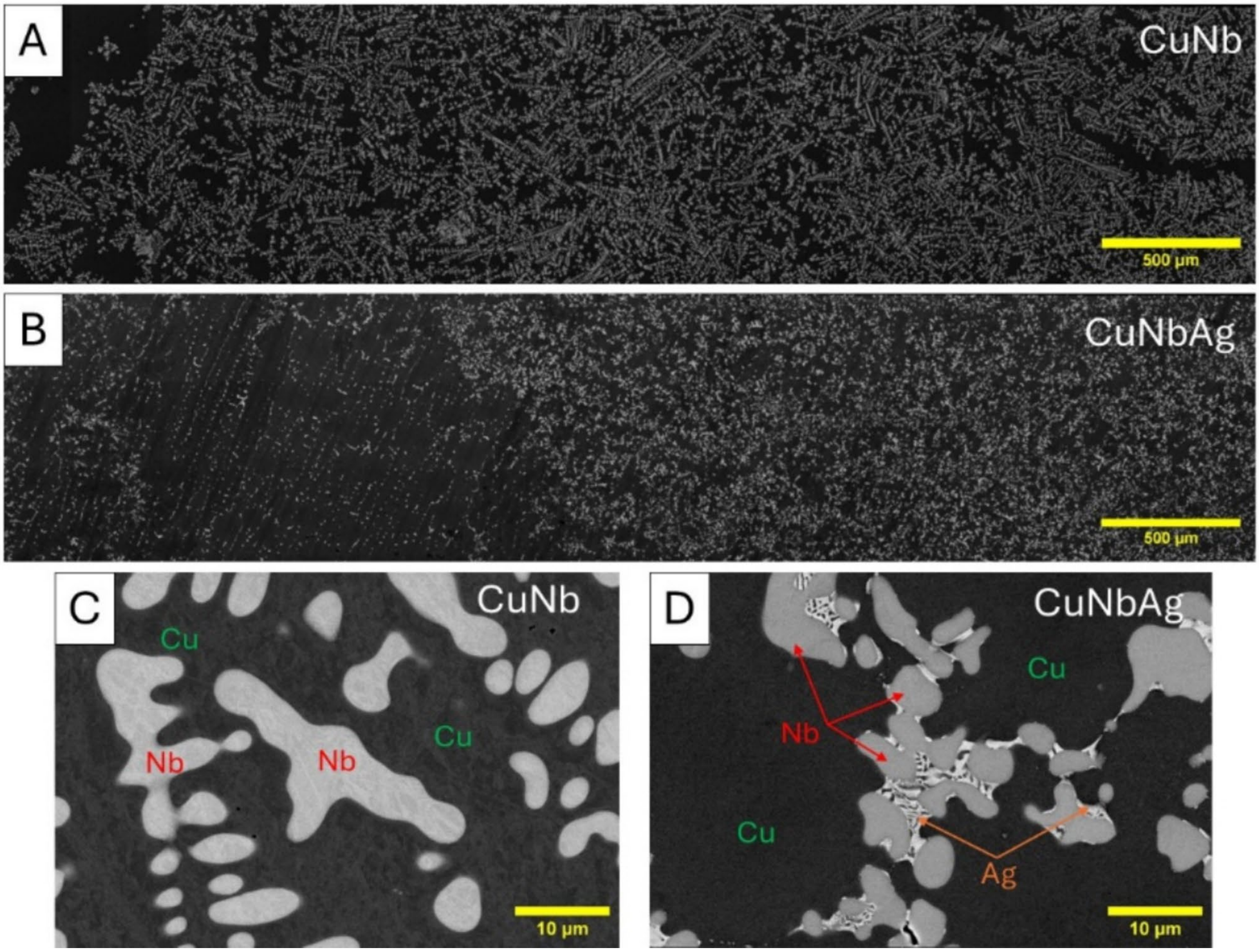

Fig. 2 Wide-field SEM mosaics of Cu-Nb (**A**) and Cu-Nb-Ag (**C**) samples, with high-magnification insets (**B and D**) highlighting Nb dendrites (bright contrast) within the Cu matrix (dark background)

temperature decreased, the solubility of the Ag in the Cu decreased. When temperature was gradually reduced, this Ag may have partially precipitated out of the matrix during the solid-state reaction, when temperature was gradually reduced.

Nb and Ag distribution

We observed distinct differences in the distribution of Nb phase in Cu-Nb and in Cu-Nb-Ag. We assumed that these differences resulted from the fact that 1) Nb content was higher in Cu-Nb than in Cu-Nb-Ag, and 2) Ag was only present in samples from the Cu-Nb-Ag ingot. In the Cu-Nb samples, Nb showed both well-developed primary and secondary dendrites, forming a typical dendritic structure, while in most areas of the Cu-Nb-Ag samples, dendritic structure was atypical.

We analyzed the morphology of Nb dendrites by calculating shape descriptors such as roundness, circularity, Feret diameter, fractal dimension, and lacunarity. These descriptors were calculated from SEM images. The data showed that Nb particles in CuNb samples were consistent with typical dendritic growth in that they were more elongated, and they exhibited more irregular boundaries than in Cu-Nb-Ag samples. By contrast, Nb particles in the Cu-Nb-Ag sample displayed shorter and more equiaxial shapes. The Cu-Nb sample showed higher fractal dimensions. The box-counting dimension (D_b) was 1.72. The dimension measured by average-based/time series methods (D_{avg}) was 1.76. These relatively high values for D_b and D_{avg} indicate that 1) complex, space-filling branched dendrites were present and 2) the interface was unstable during solidification. Cu-Nb-Ag, by contrast, had lower values for D_b and D_{avg} (1.55 and 1.54), reflecting simpler, more compact structures. It is likely that the Cu-Nb sample had a more intricate growth pattern, more dense branching, more secondary and tertiary dendrite arms, and higher solidification instability. Consequently, Cu-Nb solidified faster with relatively higher undercooling. In other

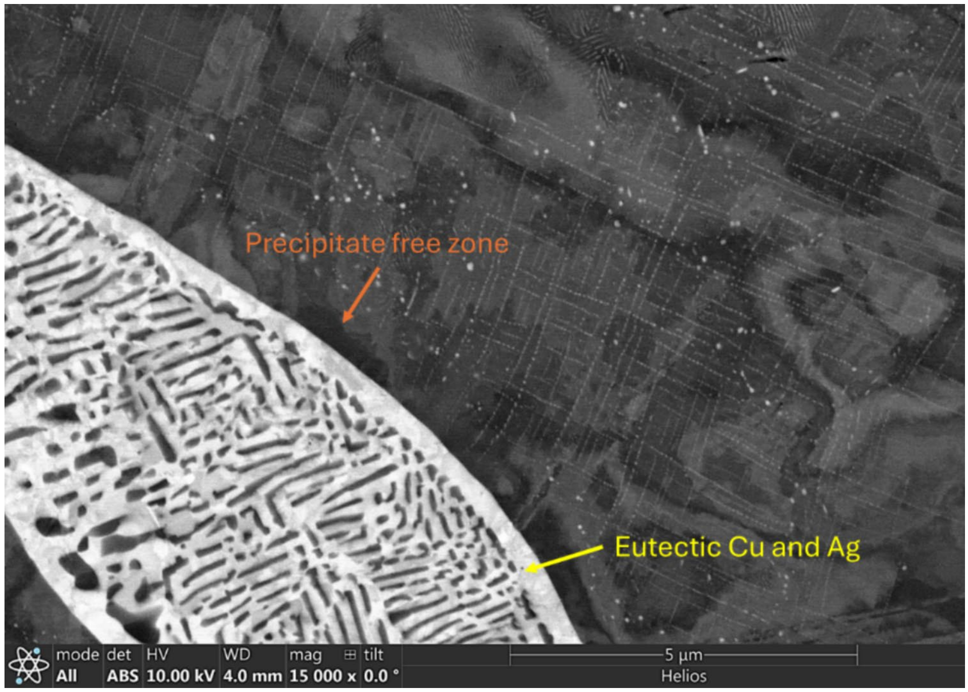

Fig. 3 SEM image taken by an angular backscattered detector (ABS) from the sample Cu-Nb-Ag. Both the eutectic product and the precipitate-free zone are marked in the figure

words, the solidification of Cu-Nb had larger thermal and/or solute gradients with stronger diffusion-limited growth.

Physically, this means the interface during solidification was more unstable, producing an intricate growth front. Although the fractal dimension of Cu-Nb-Ag was about 10% smaller than that of Cu-Nb, lacunarity in Cu-Nb-Ag (0.7) was higher than that of Cu-Nb (0.3), suggesting higher heterogeneity and greater spacing between the Nb particles (Table 1). We attributed lower fractal dimensions and higher lacunarity in Cu-Nb-Ag to the difference in Nb content and to the presence of Ag. Lower Nb content led to lower growth potential in dendrite. When Nb dendrites grow in Cu-Nb-Ag samples, they must reject both the Ag and the Cu, which means that the overall growth rate must be lower than in Cu-Nb samples. Previous work on Cu-Nb systems showed that lower Nb content alone did not produce such structure as in Cu-Nb-Ag, while ternary additions could directly modify Nb growth behavior.

Using EDS, we detected no Nb in the Cu matrices of either the Cu-Nb or the Cu-Nb-Ag samples. This is consistent with published data that the solubility of Nb in Cu is below the capability of EDS to detect it. In Cu-Nb-Ag, however, EDS was capable of detecting Ag content between 6.0 and 7.5wt% in the Cu matrix, higher than the 1–4wt% detected by light microscopy. Whatever Ag content was recognized by light microscopy, therefore, must have come from the eutectic reaction that occurred during a later stage of solidification, while whatever Ag content was detected by EDS in the Cu matrix must have come from dissolved Ag in Cu. (The data from this EDS included both the Ag remaining in the solid solution and Ag precipitates formed during the solid-state reaction, see Table 1.) Because of the low solubility of Ag in solid solution, we believe that most of Ag was in the form of precipitate particles.

In the Nb of both the Cu-Nb and the Cu-Nb-Ag samples, we detected no Cu above 1 wt% (using EDS). Cu content varied from dendrite to dendrite.

Interaction between Ag and Cu

We observed eutectic Cu-Ag products in Cu-Nb-Ag samples. Some of these eutectic products appeared to form independently from Nb (Fig. 2D), but most of them were formed by heterogeneous nucleation on Nb dendrites. The nucleation of the eutectic reaction was initiated by Ag, as evidenced by the layers of Ag formed on the surfaces of Nb dendrites.

In the eutectic regions adjacent to the Cu matrix, we observed a thick Ag layer. This indicates that, during the solidification of Cu before the eutectic reaction, Ag was rejected from the Cu, forming an Ag-rich region between the solidified Cu and the liquid alloy.

In the proeutectic Cu from the Cu-Nb-Ag samples, we observed Ag precipitates (Fig. 3). Near the eutectic region, we observed a precipitate-free-zone in the Cu matrix. From the morphology of the precipitates, we concluded that they were continuous precipitates that had formed after solidification, during a solid-state reaction. The average size of the Ag precipitates was measured to be 31 ± 7.9 nm in diameter. The spacing between the Ag precipitates within each row was about 50.7 ± 7.5 nm, and the spacing between the Ag rows was about 289.6 ± 263.7 nm.

Previous work on solidified Cu-Ag-Nb reported only that the Ag–Cu eutectic products, some of these eutectic domains solidified around the primary Nb [8, 18, 26–28]. Our work revealed Ag in both eutectic form and precipitation form. The Ag content estimated from our light microscopy images was below the nominal Ag content because the size of the Ag precipitates in the Cu was below the resolution of the light microscope we used to estimate the Ag volume fraction.

Conclusions

We compared the microstructures of solidified Cu-Nb and Cu-Nb-Ag samples. In both types of samples, our microscopy images demonstrated that the Nb dendrite formed first, before either the Cu or the Ag. In Cu-Nb, the Nb grew into a typical dendritic structure with a higher fractal dimension, while in Cu-Nb-Ag, the Nb grew into an atypical dendritic structure with a lower fractal dimension. Coarse Cu was formed only after the formation of the primary dendrites of Nb.

In Cu-Nb-Ag, large Ag particles initiated a eutectic reaction adjacent to the Nb dendrite. Fine Ag particles, leading to refined structure, formed within the Cu during a solid-state reaction. In the vicinity of the interfaces between the Cu-Ag eutectic component and the Cu matrix, we observed a precipitate-free zone in the Cu matrix and a thick Ag layer in the eutectic. These microstructural changes indicate that Ag addition to Cu-Nb not only lowers the melting point but also impacts phase distribution. This understanding provides a pathway to engineering Cu-based conductors. Quantitative shape analysis confirms that Nb in Cu-Nb is more elongated and irregular, whereas Cu-Nb-Ag contains shorter and more equiaxial Nb morphologies.

Acknowledgments A portion of the work was performed at the National High Magnetic Field Laboratory, which is supported by National Science Foundation Cooperative Agreement No. DMR-2128556 and DMR-1839796, and the State of Florida. We thank Mary Tyler for editing and Peter Chupas for discussion.

Author contributions Hannah Matos-Pimentel (HMP) conducted microscopy work. Matthew Besser (MB) and Ryan Timothy Ott were responsible for producing the ingots, with MB providing the fabrication conditions. Ke Han (KH) designed the experiment. HMP and KH performed the data analysis and wrote the manuscript.

Funding This Study was funded by National Science Foundation, DMR-2128556, DMR-1839796.

Data availability The data supporting the findings of this study are available from the corresponding author upon reasonable request.

Declarations

Conflict of interest On behalf of all authors, the corresponding author states that there is no conflict of interest. AI-assisted image generation tools were used solely for the preparation of the graphical abstract. No AI tools were used in the generation, modification, or analysis of the experimental data.

References

1. K. Han, J. Embury, J. Sims, L. Campbell, H.-J. Schneider-Muntau, V. Pantsyrnyi, A. Shikov, A. Nikulin, A. Vorobieva, The fabrication, properties and microstructure of Cu–Ag and Cu–Nb composite conductors. Mater. Sci. Eng. A **267**(1), 99–114 (1999)
2. K. Han, J. Lu, V. Toplosky, R. Niu, R. Goddard, Y. Xin, R. Walsh, I. Dixon, V. Pantsyrny, Properties of selected high-strength composite conductors with different strengthening components. IEEE Trans. Appl. Supercond. **30**(4), 4301305 (2020)
3. K. Han, V.J. Toplosky, Y. Xin, J.R. Sims, C.A. Swenson, Fatigue property examinations of conductors for pulsed magnets. IEEE Trans. Appl. Supercond. **20**(3), 1463–1466 (2010)
4. J.R. Sims, J.B. Schillig, C.A. Swenson, D.L. Gardner, A.N. Matlashov, C.N. Ammerman, Low-noise pulsed pre-polarization magnet systems for ultra-low field NMR. IEEE Trans. Appl. Supercond. **20**(3), 752–755 (2010)
5. C.A. Swenson, A.V. Gavrilin, K. Han, R.P. Walsh, H.J. Schneider-Muntau, D.G. Rickel, J.B. Schillig, C.N. Ammerman, J.R. Sims, Performance of 75 T prototype pulsed magnet. IEEE Trans. Appl. Supercond. **16**(2), 1650–1655 (2006)
6. C.A. Swenson, W.S. Marshall, A.V. Gavrilin, K. Han, J. Schillig, J.R. Sims, H.J. Schneider-Muntau, Progress of the insert coil for the US-NHMFL 100T multi-shot pulse magnet. Physica B-Condensed Matter. **346**, 561–565 (2004)
7. V. Pantsyrny, A. Shikov, A. Vorobieva, Nb3Sn material development in Russia. Cryogenics **48**(7–8), 354–370 (2008)
8. D. Raabe, S. Ohsaki, K. Hono, Mechanical alloying and amorphization in Cu-Nb-Ag in situ composite wires studied by transmission electron microscopy and atom probe tomography. Acta Mater. **57**(17), 5254–5263 (2009)
9. W.A. Spitzig, H.L. Downing, F.C. Laabs, E.D. Gibson, J.D. Verhoeven, Strength and electrical-conductivity of a deformation-processed Cu-5 pct Nb composite. Metall. Trans. A **24**(1), 7–14 (1993)
10. Y. Sakai, H.J. SchneiderMuntau, Ultra-high strength, high conductivity Cu-Ag alloy wires. Acta Mater. **45**(3), 1017–1023 (1997)
11. T.D. Shen, X. Zhang, K. Han, C.A. Davy, D. Aujla, P.N. Kalu, R.B. Schwarz, Structure and properties of bulk nanostructured alloys synthesized by flux-melting. J. Mater. Sci. **42**(5), 1638–1648 (2007)

12. K.X. Song, Y.F. Geng, Y.J. Ban, Y. Zhang, Z. Li, X.J. Mi, J. Cao, Y.J. Zhou, X.B. Zhang, Effects of strain rates on dynamic deformation behavior of Cu-20Ag alloy. J. Mater. Sci. Technol. **79**, 75–87 (2021)
13. B. An, R. Niu, Y. Xin, W.L. Starch, Z. Xiang, Y. Su, R.E. Goddard, J. Lu, T.M. Siegrist, E. Wang, Suppression of discontinuous precipitation and strength improvement by Sc doping in Cu-6 wt% Ag alloys. J. Mater. Sci. Technol. **135**, 80–96 (2023)
14. B. An, Y. Xin, R. Niu, J. Lu, E. Wang, K. Han, Hardening Cu-Ag composite by doping with Sc. Mater. Lett. **252**, 207–210 (2019)
15. B. An, Y. Xin, R. Niu, Z. Xiang, Y. Su, J. Lu, E. Wang, K. Han, Stacking fault formation and Ag precipitation in Cu-Ag-Sc alloys. Mater Charact **189**, 111965 (2022)
16. B. An, Y. Xin, R. Niu, Z. Xiang, E. Wang, K. Han, Nucleation and growth of discontinuous precipitates in Cu–Ag alloys. Mater. Res. Exp. **9**(2), 026530 (2022)
17. C.C. Zhao, X.W. Zuo, E.G. Wang, K. Han, Strength of Cu-28 wt%Ag composite solidified under high magnetic field followed by cold drawing. Met. Mater. Int. **23**(2), 369–377 (2017)
18. C. Zhao, X. Zuo, E. Wang, R. Niu, K. Han, Simultaneously increasing strength and electrical conductivity in nanostructured Cu–Ag composite. Mater. Sci. Eng. A **652**, 296–304 (2016)
19. X.W. Zuo, K. Han, C.C. Zhao, R.M. Niu, E.G. Wang, Microstructure and properties of nanostructured Cu28 wt%Ag microcomposite deformed after solidifying under a high magnetic field. Materials Science and Engineering: A. **619**, 319–327 (2014)
20. X.W. Zuo, C.C. Zhao, E.G. Wang, L. Zhang, K. Han, J.C. He, Microstructure evolution of the proeutectic Cu dendrites in diamagnetic Cu-Ag Alloys by electromagnetic suppressing convection. J. Low Temp. Phys. **170**(5–6), 409–417 (2013)
21. N. Ageew, M. Hansen, G. Sachs, Segregation and property changes supersaturated silver-copper alloys. Z. Phys. **66**(5–6), 350–376 (1930)
22. R.A. Fournelle, J.B. Clark, Genesis of cellular precipitation reaction. Metall. Trans. **3**(11), 2757–2767 (1972)
23. J. Freudenberger, A. Kauffmann, H. Klauss, T. Marr, K. Nenkov, V.S. Sarma, L. Schultz, Studies on recrystallization of single-phase copper alloys by resistance measurements. Acta Mater. **58**(7), 2324–2329 (2010)
24. A. Gaganov, J. Freudenberger, E. Botcharova, L. Schultz, Effect of Zr additions on the microstructure, and the mechanical and electrical properties of Cu-7 wt.%Ag alloys. Mater. Sci. Eng. A **437**(2), 313–322 (2006)
25. A. Gaganov, J. Freudenberger, W. Grunberger, L. Schultz, Microstructural evolution and its effect on the mechanical properties of Cu-Ag microcomposites. Z. Metallkd. **95**(6), 425–432 (2004)
26. D. Raabe, D. Mattissen, Microstructure and mechanical properties of a cast and wire-drawn ternary Cu-Ag-Nb in situ composite. Acta Mater. **46**(16), 5973–5984 (1998)
27. D. Raabe, D. Mattissen, Experimental investigation and Ginzburg-Landau modeling of the microstructure dependence of superconductivity in Cu-Ag-Nb wires. Acta Mater. **47**(3), 769–777 (1999)
28. C. Zhao, R. Niu, Y. Xin, D. Brown, D. McGuire, E. Wang, K. Han, Improvement of properties in Cu–Ag composites by doping induced microstructural refinement. Mater. Sci. Eng. A **799**, 140091 (2021)
29. I. Arganda-Carreras, V. Kaynig, C. Rueden, K.W. Eliceiri, J. Schindelin, A. Cardona, H.S. Seung, Trainable Weka segmentation: a machine learning tool for microscopy pixel classification. Bioinformatics **33**(15), 2424–2426 (2017)